Available online at www.sciencedirect.com

ScienceDirect

Ceramics International 40 (2014) 3887–3893

CERAMICS INTERNATIONAL

www.elsevier.com/locate/ceramint

Enhancement of the photocatalytic performance of Ni-loaded TiO_2 photocatalyst under sunlight

Yanhua Liu, Zilong Wang, Weibo Fan, Zhongrong Geng, Libang Feng*

School of Mechatronic Engineering, Lanzhou Jiaotong University, Lanzhou 730070, China

Received 15 July 2013; received in revised form 6 August 2013; accepted 6 August 2013
Available online 13 August 2013

Abstract

A highly sunlight active Ni-loaded TiO_2 nanocomposite (Ni/TiO_2) is successfully prepared by a simple chemical reduction method using tetrabutyl titanate as a precursor, $Ni(NO_3)_2 \cdot 6H_2O$ as a nickel source, and $N_2H_4 \cdot H_2O$ as a reductant, respectively. The crystal structure, morphology and UV–vis diffuse reflectance characteristics are investigated by XRD, TEM, and UV–vis diffuse reflectance spectroscopy, while the photocatalytic performance of Ni/TiO_2 is evaluated by photocatalytic degradation of methyl orange solution under UV and sunlight irradiation. Results show that the crystal structure of TiO_2 is not changed upon the loading of Ni, the photocatalytic performance of TiO_2 under both UV-light and sunlight, however, is enhanced greatly. The enhancement of the photocatalytic performance of Ni/TiO_2 is attributed to the increase of the photogenerated electron–hole separation efficiency and the advanced absorption of light due to surface plasmon effect of Ni nanoparticles.

Keywords: Ni loading; Ni/TiO_2 nanocomposites; Photocatalytic activity; Mechanism

1. Introduction

The existence of organic pollutes in water and wastewater is a primary cause of serious pollution problems which can influence human health, and there requires a complete removal of these toxic and carcinogenic organic dyes [1,2]. Anatase phase of TiO_2 is the most preferable photocatalyst that extensively used in degradation and mineralization of organic dyes due to its high efficiency, strong oxidizing power, non-toxicity, high photochemical stability, and low cost [3]. However, the photocatalytic efficiency of TiO_2 is hampered by the main drawback of rapid recombination of photo-generated electron–hole pairs. To avoid the limitation, the modification of TiO_2 with metal nanoparticles is an effective technology to obtain more efficient photocatalytic activity. Several research workers have reported that loading some effective noble metals, especially Au, Ag, and Pt nanoparticles, on the surface of TiO_2 can significantly enhance the photocatalytic performance of TiO_2 [4–8]. However, such precious metals are very expensive in the view point of practical application. In addition, some authors have employed effective non-precious transition metals, including Fe [9,10], Cu [11,12], Cr [13], Mn [14], Co, W [15], and so on, to synthesize composite for the enhancement of photocatalytic activity of TiO_2.

Ni nanoparticles, especially supported Ni nanoparticles on various carriers, have been extensively studied for the catalytic activity enhancement [16–19]. Recently, Ni/TiO_2 composite has been studied. For instance, Wu et al. has prepared Ni/TiO_2 nanocomposite by electroless plating technique for selective hydrogenation of p-nitrophenol to p-aminopheol [20]. However, the synthetic method they adopted is slightly complicated. Meanwhile, the photocatalytic activity has not been studied. In order to enhance the photocatalytic performance of TiO_2 both under UV and sunlight, in this paper, Ni-loaded TiO_2 nanocomposite is prepared by a simple chemical reduction method, and the photocatalytic activity of Ni/TiO_2 has been evaluated. Results show that the photocatalytic activity of TiO_2 has been improved greatly by Ni loading under both UV-light and sunlight irradiation.

2. Experimental

2.1. Synthesis of TiO_2 nanoparticles

TiO_2 nanoparticles were synthesized by the sol–gel method [21,22] using tetrabutyl titanate (TBT) as a precursor. The as-prepared

*Corresponding author. Tel.: +86 931 495 7092; fax: +86 931 493 8043.
E-mail address: lepond@hotmail.com (L. Feng).

0272-8842/$ - see front matter © 2013 Elsevier Ltd and Techna Group S.r.l. All rights reserved.
http://dx.doi.org/10.1016/j.ceramint.2013.08.030

TiO_2 nanoparticles were annealed at 500 °C for 2 h to convert the amorphous TiO_2 to the crystalline form.

2.2. Preparation of Ni-loaded TiO_2 (Ni/TiO_2)

The Ni-loaded TiO_2 (Ni/TiO_2) photocatalyst was prepared according to the following steps: Firstly, the as-annealed TiO_2 nanoparticles were suspended in 50 mL distilled water and sonicated for 1 h to well disperse the nanoparticles. Then $N_2H_4 \cdot H_2O$ was charged into the suspension and sonicated for 10 min. Second, the solution containing 5 mg of $AgNO_3$ (notes: which is used as nucleation sites) and the required amount of $Ni(NO_3)_2 \cdot 6H_2O$ was added dropwise, in which the added amount of Ni was x, and x=3%, 6%, 9% and 12%, calculated theoretically as molar ratio of loaded Ni and TiO_2 ($x=n$(Ni): $n(TiO_2)$). The solution was kept reaction for 2 h with stirring after the Ni solution was dripped off. During the reaction, the color of the suspension gradually turned gray, indicating Ni^{2+} has been reduction to Ni. Finally, the obtained powder was separated from the suspension by centrifugation under 1500 rpm, and washed for three times with distilled water and ethanol. Then the resulting product was dried at 60 °C for 24 h.

2.3. Photocatalytic activity investigation and evaluation

The photocatalytic activity of TiO_2 and Ni/TiO_2 was evaluated by monitoring the photodegradation of methyl orange (MO) in aqueous solution, respectively. 0.20 g of photocatalyst of TiO_2 or Ni/TiO_2 was charged into 50 mL of 10 mg/L MO aqueous solution, respectively. The mixed solution was irradiated using high-pressure mercury lamp (λ_{max}=365 nm) under stirring. Samples were then taken out every 30 min and the photocatalyst was separated from the mixture solution by centrifugation immediately, and then the UV–vis absorption of the clarified solution was analyzed with a UV–vis spectrometer (UV-2550, Shimadzu). The absorbance of MO solution was measured at a wavelength of 465 nm, which corresponds to the maximum absorption wavelength of MO.

The photocatalytic activity of TiO_2 and Ni/TiO_2 was also investigated under sunlight irradiation. 0.20 g of photocatalyst of TiO_2 or Ni/TiO_2 was charged into 50 mL of 10 mg/L MO aqueous solution, respectively. The mixed solution was irradiated using sunlight under stirring. Samples were then taken out every 5 min and the photocatalyst was separated from the mixture solution by centrifugation immediately, and then the UV–vis absorption of the clarified solution was analyzed with a UV–vis spectrometer (UV-2550, Shimadzu). The absorbance of MO solution was measured at 465 nm, which corresponds to the maximum absorption wavelength of MO.

2.4. Characterization

The morphology was observed with transmission electron microscopy (TEM, Tecnai G2F30), the X-ray diffraction (XRD) patterns were measured using a X-ray diffractometer (XRD-7000, Shimadzu), and the UV–vis diffuse reflectance spectra were characterized with a UV–vis spectrometer (UV-2550, Shimadzu).

3. Results and discussion

3.1. Structure of Ni/TiO_2

X-ray diffraction patterns of TiO_2 and Ni/TiO_2 are presented in Fig. 1. The diffraction pattern of TiO_2 agrees well with that in JCPDS 21-1272 card for TiO_2. The diffraction peaks present at 25.4°, 37.6°, and 48.2° are typical patters of anatase, which contribute to the (101), (004) and (200) crystal plane, respectively. It can also be seen from Fig. 1 that both pure TiO_2 and TiO_2 in Ni/TiO_2 present in anatase phase, while the loading of Ni does not influence the crystallization performance of TiO_2. In addition, the reflection peak of Ni in Ni/TiO_2 presents at 2θ=44.6°, which is marked with an asterisk, and it accords well with that in JCPDS 04-0850 card for Ni with face centered cubic (FCC) structure. The reflection peak corresponds to the Ni (111) crystal plane, manifesting that Ni has been loaded on TiO_2 successfully.

3.2. Morphology of Ni/TiO_2

The morphology of TiO_2 and Ni/TiO_2 is displayed in Fig. 2. The morphology of TiO_2 (see Fig. 2a) indicates that TiO_2 after annealing have sheet structure and agglomerate to some degree to form particles with 20–40 nm in size. The morphology of Ni/TiO_2 (x=6%) (as shown in Fig. 2b) displays that spherical Ni nanoparticles with around 10–20 nm in size are clearly dispersed on the external surface of TiO_2 nanoparticles. Because of the difference in electron density, TiO_2 and Ni nanoparticles are distinguishable and thus Ni nanoparticles can be identified as dark spots on TiO_2 nanoparticles.

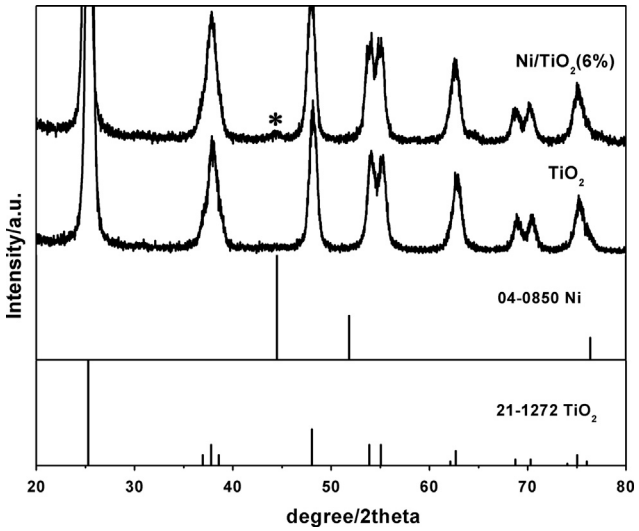

Fig. 1. XRD patterns of TiO_2 and Ni/TiO_2 (x=6%).

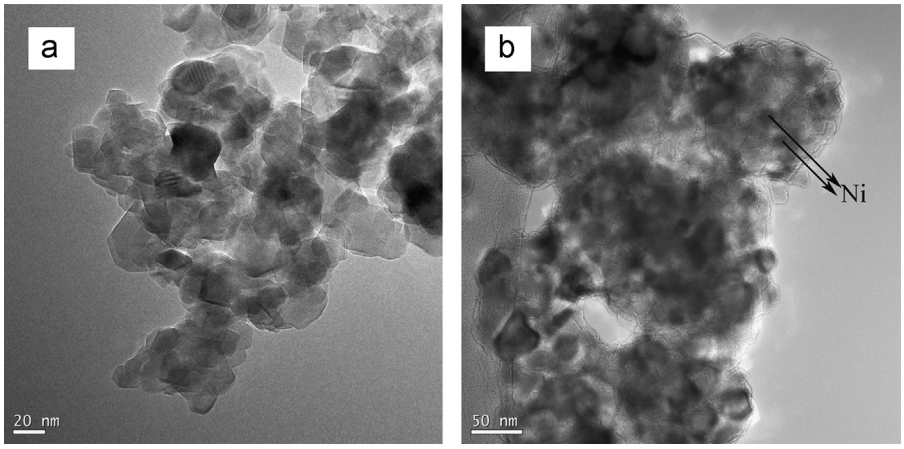

Fig. 2. TEM images of (a) TiO_2 and (b) Ni/TiO_2 (x=6%).

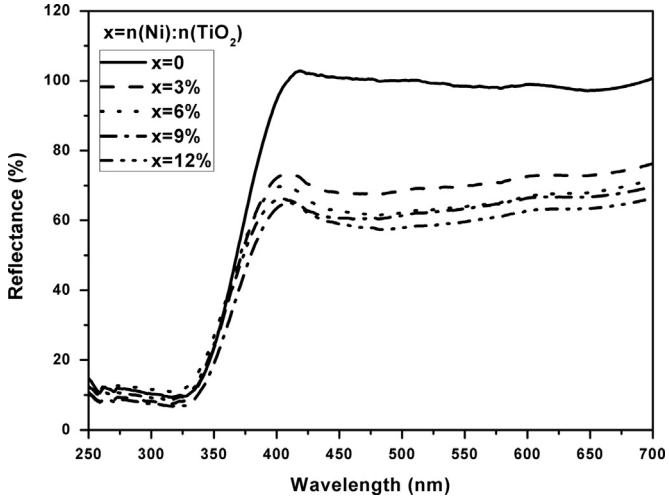

Fig. 3. UV–vis diffuse reflectance spectra of TiO_2 and Ni/TiO_2 composites.

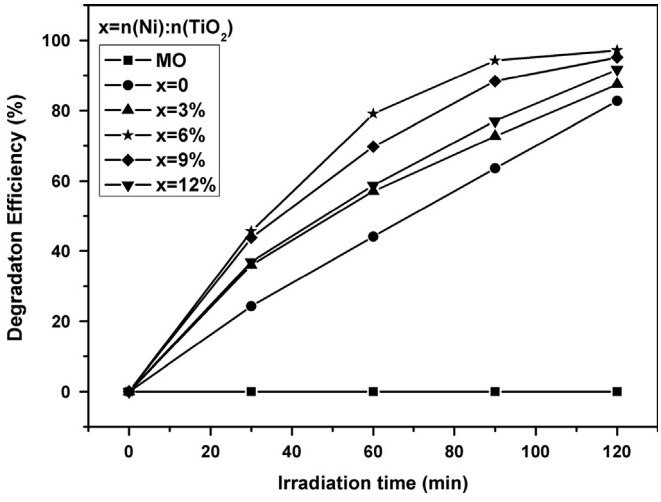

Fig. 4. Photocatalytic degradation efficiency of MO under UV irradiation over TiO_2 and Ni/TiO_2.

3.3. UV–vis diffuse reflectance spectra of Ni/TiO_2

Fig. 3 displays the UV–vis diffuse reflectance spectra of pure titanium oxide and the samples loaded with various nickel contents. The spectra show a definite band edge in the UV region ranging from 340 nm to 400 nm which attributed to photo excitation from valence band to conduction band. It can be clearly seen that Ni/TiO_2 nanocomposites with different nickel contents can significant exhibit a continuous and stronger absorption band than that of pure TiO_2 at the range of 400–700 nm, which could be attributed to the surface plasmon resonance (SPR) of Ni nanoparticles.

The band gap energies (E_g) are obtained from the wavelength values corresponding to the intersection point of the vertical and horizontal parts of the spectra using the equation

$$E_g = \frac{hc}{\lambda} \quad (1)$$

where E_g is the band gap energy (eV), h is Plank's constant, c the light velocity (m/s), and λ the wavelength (nm). The obtained values of E_g are 3.43, 3.42, 3.40, 3.41 and 3.42 eV for the pure TiO_2 and the Ni/TiO_2 loaded with 3%, 6%, 9%, 12% nickel, respectively, which suggested that nickel loading does not change the band gap energy of TiO_2. Therefore, the red shift of wavelength is not contributed to the change of band gap, but it resulted from the absorption of nickel nanopowder in the visible region due to the SPR effect of Ni nanoparticles.

3.4. Photocatalytic performance of Ni/TiO_2 under UV-light irradiation

Methyl orange (MO) was used as a model dye to estimate the photocatalytic activity of Ni/TiO_2 under UV-light irradiation. The photocatalytic degradation efficiency of aqueous MO with TiO_2 and Ni/TiO_2 was calculated and illustrated in Fig. 4, which depicts the variation of photocatalytic activity of TiO_2 and Ni/TiO_2 at the maximal absorption wavelength of MO (namely, 465 nm) with the irradiation time. It can be found from Fig. 4 that all the Ni/TiO_2 exhibit higher photocatalytic activity as compared with TiO_2. Moreover, with increasing the molar ratio of Ni to TiO_2 from 3% to 12%, the photocatalytic activity increases at first and then decreases. Meanwhile, the photocatalytic activity of Ni/TiO_2

reaches the highest while the molar ratio of Ni to TiO_2 arrives at 6%, and MO can be completely degraded at this optimum Ni loading.

Fig. 5 illustrates the UV–vis absorption spectra of aqueous MO during the photodegradation under UV irradiation over TiO_2 and Ni/TiO_2 (x=6%), respectively. As compared with the absorbance of system catalyzed with pure TiO_2 (see Fig. 5a), the degradation efficiency in the system catalyzed with Ni/TiO_2 (x=6%) increases greatly and MO can be degraded quickly as reaction time goes on, as shown in Fig. 5b. Moreover, it can be seen from Fig. 5b that the absorbance of MO almost reaches zero after 2 h, confirming that the as-prepared Ni/TiO_2 has outstanding photocatalytic performance.

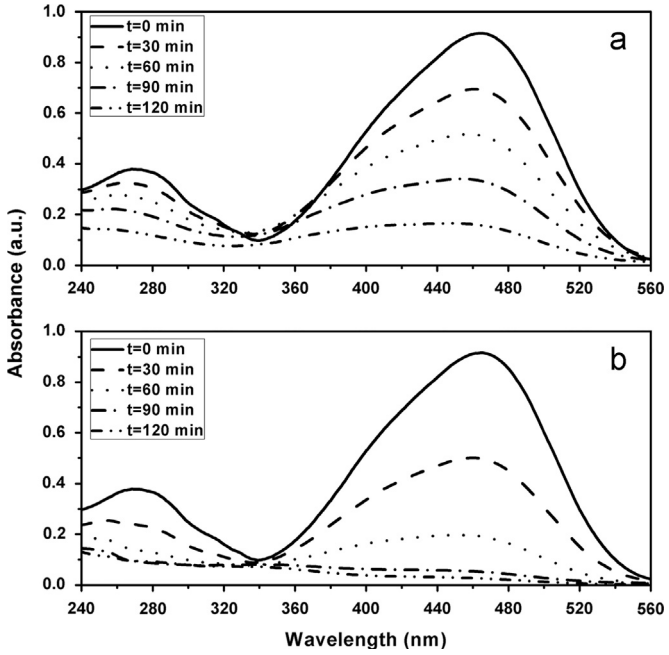

Fig. 5. Photodegradation of MO under UV irradiation catalyzed with (a) TiO_2 and (b) Ni/TiO_2 (x=6%).

The kinetics of MO photodegradation on the photocatalyst surface can be described by the first-order reaction

$$\ln\frac{C_0}{C_t} = kt \quad (2)$$

where k is the rate constant (min^{-1}), C_0 is the initial concentration of MO and C_t is the concentration of MO at the irradiation time (t). In Fig. 6, the linear relation of $\ln(C_0/C_t)$ versus irradiation time (t) for MO is presented. Rate constants are determined for all tested photocatalysts from the slope of linear fitting line and the intercept is equal to zero, as showed in Fig. 6. Meanwhile, the linear relationship between $\ln(C_0/C_t)$ and (t) indicates that the photodegradation reaction also follows the pseudo first-order reaction. Table 1 listed the rate constants for MO decomposition on all investigated photocatalysts. It can be seen that the rate constants of Ni/TiO_2 are higher than that of pure TiO_2, and the rate constant is near triple for the sample Ni/TiO_2 (x=6%) compared with pure TiO_2.

3.5. Photocatalytic performance of Ni/TiO_2 under sunlight irradiation

Fig. 7 shows the comparison of the photocatalytic activities of TiO_2 and Ni/TiO_2 under sunlight irradiation. It can be clearly seen that it cannot take about 30 min to decompound the MO completely using pure TiO_2 as photocatalyst.

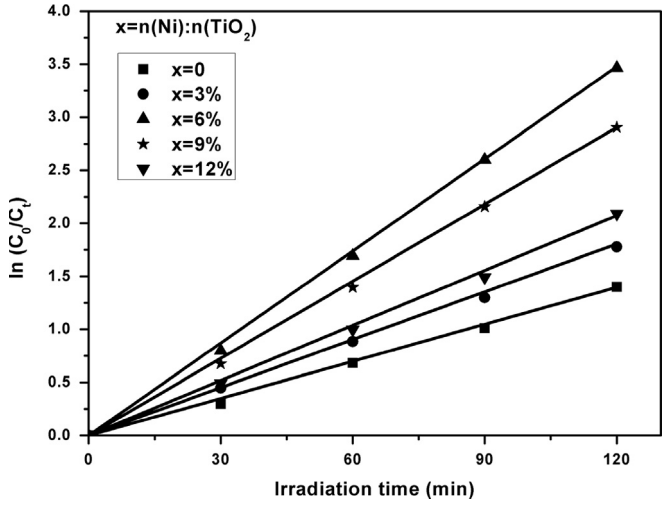

Fig. 6. Kinetic data for the degradation of aqueous MO under UV irradiation over TiO_2 and Ni/TiO_2.

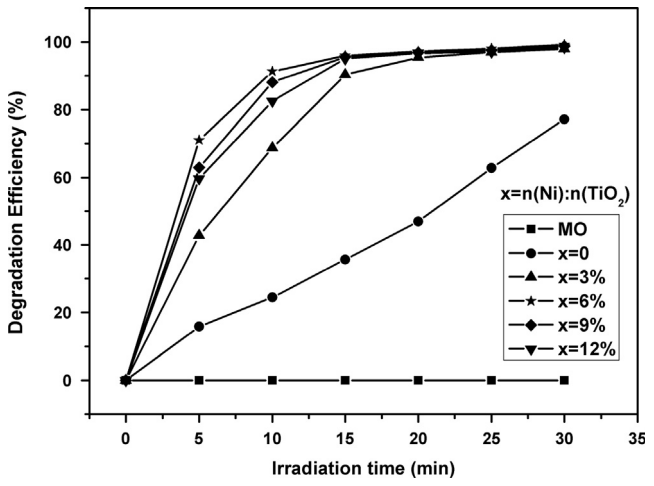

Fig. 7. Photocatalytic degradation efficiency of MO under sunlight irradiation over TiO_2 and Ni/TiO_2.

Table 1
Rate constants of MO photodegradation for neat TiO_2 and Ni/TiO_2 under UV-light irradiation.

Photocatalysts	Pure TiO_2	x=3%	x=6%	x=9%	x=12%
k (min^{-1})	0.01164	0.01504	0.02897	0.02421	0.01728

However, for the Ni/TiO_2 nanocomposites, the total time decreases to less than 20 min to decompound MO solution. Especially, for the sample loaded with 6% nickel, the total time needed to decompound MO solution decreases to 15 min. If the content of Ni either increases or decreases, the photocatalytic performance will degenerate slightly, though they are still much better than pure TiO_2.

Fig. 8 illustrates the UV–vis absorption spectra of aqueous MO during the photodegradation under sunlight irradiation over TiO_2 and Ni/TiO_2 (x=6%), respectively. As compared with the absorbance of system catalyzed with pure TiO_2 (see Fig. 8a), the degradation efficiency in the system catalyzed with Ni/TiO_2 (x=6%) increases greatly and MO can be degraded quickly as reaction time goes on, as shown in Fig. 8b. Moreover, it can be seen from Fig. 8b that the absorbance of MO almost reaches zero after 15 min, confirming that the as-prepared Ni/TiO_2 has more outstanding photocatalytic performance under sunlight.

In Fig. 9, the linear relation of $\ln(C_0/C_t)$ versus irradiation time (t) for MO is presented. Rate constants are determined for all tested photocatalysts from the slope of linear fitting line and the intercept is equal to zero, as showed in Fig. 9. Meanwhile, the linear relationship between $\ln(C_0/C_t)$ and (t) indicates that the photodegradation reaction also follows the pseudo first-order reaction. Table 2 listed the rate constants for MO decomposition on all investigated photocatalysts. It can be seen that the rate constants of Ni/TiO_2 are higher than that of pure TiO_2, and the rate constant is near triple for the sample Ni/TiO_2 (x=6%) compared with pure TiO_2.

3.6. Mechanism of the photocatalytic performance enhancement

The photocatalytic activity of anatase in degradation process is usually influenced by electron–hole recombination rate.

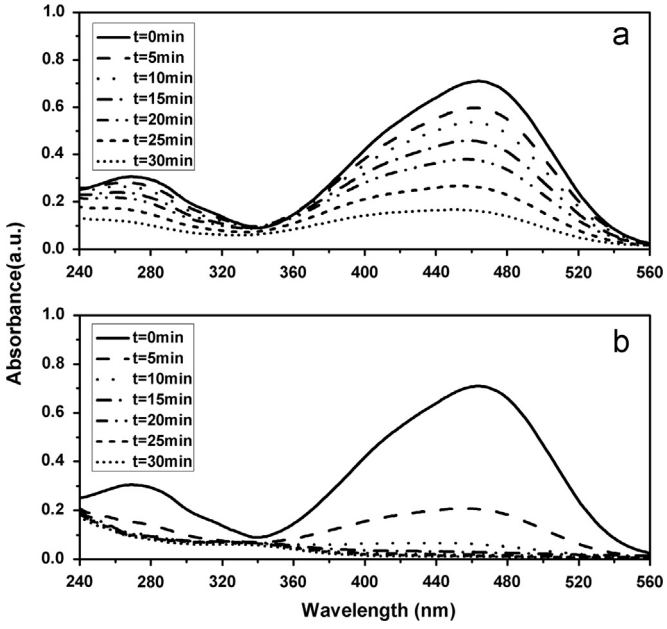

Fig. 8. Photodegradation of MO under sunlight irradiation catalyzed with (a) TiO_2 and (b) Ni/TiO_2 (x=6%).

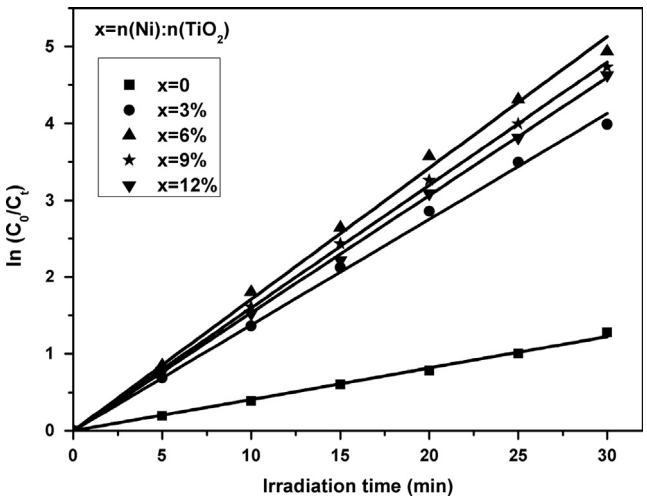

Fig. 9. Kinetic data for the degradation of aqueous MO under sunlight irradiation over TiO_2 and Ni/TiO_2.

As far as Ni/TiO_2 is concerned, Ni nanoparticles supported at TiO_2 surface can be regarded as receiving device for photo-induced electrons, which can accelerate transfer rate of electrons to oxygen and decrease the recombination rate of e^-–h^+.

Photocatalytic activity changing with the amount of Ni loading is due to the increased particle size which can change the energy level structure of Ni nanoparticles [23]. The relative vacuum energy levels of TiO_2, Ni and molecular oxygen absorbed on TiO_2 are displayed in Fig. 10. The energy level of the conduction band (CB) of TiO_2 is −4.4 eV. In order to effectively accept the photo-induced electrons, the energy level of Ni nanoparticles must lower than −4.4 eV. The energy level of Ni nanoparticles are closely related with its size [23], and which varies from −1.156 eV for single Ni atom (n=1) to −5.15 eV for Ni bulk. Along with the increasing of the size of Ni nanoparticles, the energy level of Ni nanoparticles will decrease below −4.4 eV and begin to effectively accept photo-generated electrons (see Eq. (2)). Simultaneously, these electrons can be transferred to molecular oxygen on TiO_2 and more molecular oxygen can be reduced to superoxide anion ($^{\bullet}O_2^-$), which can availably decrease the recombination of electron–hole and increase the production of superoxide anion ($^{\bullet}O_2^-$). As a result, the photocatalytic property is enhanced.

When the size of Ni nanoparticles increases to some extent (the amount of Ni loading is 6%, as showed in Fig. 4), the energy level of Ni nanoparticles is as same as that of molecular oxygen on TiO_2, and the photocatalytic property of Ni/TiO_2 reaches an optimal state. When Ni_n increases further, its energy level changes to lower than that of O_2 on the surface of TiO_2. Consequently, Ni nanoparticles cannot migrate electrons to the oxygen absorbed on TiO_2 though it still serves as photo-induced electron accepter, which causes the reduction of superoxide anion ($^{\bullet}O_2^-$) and leads to the degradation of photocatalytic performance.

The relationship between the effect of Ni and its loaded amount may be explained as follows:

$$e^- + Ni_n \rightarrow Ni_n^- \quad (3)$$

Table 2
Rate constants of MO photodegradation for neat TiO_2 and Ni/TiO_2 under sunlight irradiation.

Photocatalysts	Pure TiO_2	$x=3\%$	$x=6\%$	$x=9\%$	$x=12\%$
k (min^{-1})	0.0408	0.1376	0.1710	0.1598	0.1532

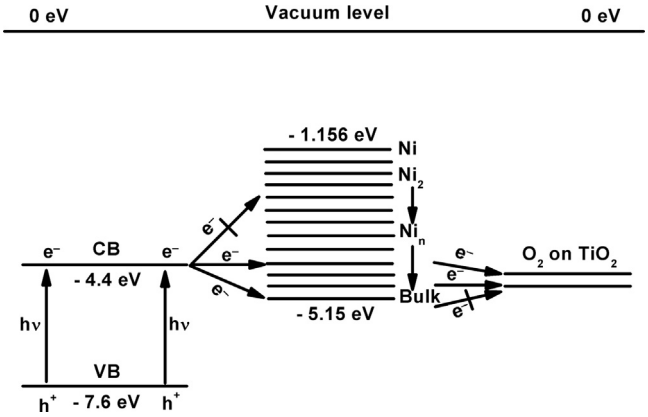

Fig. 10. Schematic diagram of the transfer of photoinduced electrons on the interface of Ni/TiO_2 (means incapable).

$$Ni_n^- + O_2 \rightarrow Ni_n + {}^{\bullet}O_2^- \quad (4)$$

$$Ni_n^- + h^+ \rightarrow Ni_n \quad (5)$$

With the size increasing of Ni nanoparticles, its energy level is close to Ni bulk, and then the reaction (5) competes with reaction (4). Thus, Ni nanoparticles can become recombination center of photo-generated electron–hole pairs, which will lead to the decrease of photocatalytic performance.

Additionally, the photocatalytic performance of Ni/TiO_2 irradiated by sunlight is better than that irradiated by UV-light. A possible explanation is as follows: the absorption of visible light (as showed in Fig. 3) due to the surface plasmon effect of Ni nanoparticles also resulted in the enhancement of photocatalytic activity, because the excited electrons in Ni nanoparticles transfer to the surface of TiO_2 under visible irradiation [8,24], and these electrons may also react with oxygen absorbed on the surface of TiO_2 to produce oxygen radicals ($^{\bullet}O_2^-$), which are able to promote the photocatalytic reaction progress greatly in the visible region. Together, Ni/TiO_2 nanocomposites exhibit excellent photocatalytic performance under the UV region included in sunlight. Hence, Ni/TiO_2 nanocomposites have better photocatalytic performance under sunlight.

4. Conclusions

The Ni-loaded TiO_2 nanocomposite (Ni/TiO_2) was prepared by a simple chemical reduction method using $N_2H_4 \cdot H_2O$ as a reductant. Ni/TiO_2 shows better photocatalytic activity than that of TiO_2 on the degradation of methyl orange under both UV irradiation and sunlight irradiation. Additionally, the photocatalytic performance of Ni/TiO_2 irradiated by sunlight is better than that irradiated by UV-light due to the surface plasmon effect of Ni nanoparticles. Moreover, Ni/TiO_2 loaded 6% molar content of Ni has the highest photodegradation efficiency for complete degradation of MO. As compared to TiO_2, the outstanding photocatalytic performance of Ni/TiO_2 was attributed to the high photo-generated electron–hole separation efficiency and the advanced absorption of light due to surface plasmon effect of Ni nanoparticles.

Acknowledgments

This work is financially supported by Advanced Research Foundation of Jinchuan Group Ltd. (No. 420032) and National Natural Science Foundation of China (No. 11104126).

References

[1] S. Ahmed, M.G. Rasul, R. Brown, M.A. Hashib, J. Environ, Influence of parameters on the heterogeneous photocatalytic degradation of pesticides and phenolic contaminants in wastewater: A short review, Journal of Environmental Management 92 (2011) 311–330.
[2] Q.Z. Luo, X.Y. Li, X.Y. Li, D.S. Wang, J. An, X.X. Li, Visible light photocatalytic activity of TiO_2 nanoparticles modified by pre-oxidized polyacrylonitrile, Catalysis Communications 26 (2012) 239–243.
[3] M.A. Ahmed, Synthesis and structural features of mesoporous NiO/TiO_2 nanocomposites prepared by sol–gel method for photodegradation of methylene blue dye, Journal of Photochemistry and Photobiology A 238 (2012) 63–70.
[4] J.W. Zhang, M. Zhang, Z.S. Jin, J.J. Wang, Z.J. Zhang, Study of high-temperature hydrogen reduced Pt^0/TiO_2 by X-ray photoelectron spectroscopy combined with argon ion sputtering–diffusion-encapsulation effect in relation to strong metal-support interaction, Applied Surface Science 258 (2012) 3991–3999.
[5] H.H. Wang, J.L. Faria, S.J. Dong, Y. Chang, Mesoporous Au/TiO_2 composites preparation, characterization, and photocatalytic properties, Materials Science and Engineering B 177 (2012) 913–919.
[6] E. Pulido Melián, O. González Díaz, J.M. Doña Rodríguez, G. Colón, J.A. Navío, M. Macías, J. Pérez Peña, Effect of deposition of silver on structural characteristics and photoactivity of TiO_2-based photocatalysts, Applied Catalysis B: Environmental 127 (2012) 112–120.
[7] M.Y. Li, R.X. Wang, P. Zhong, X.K. Li, Z.P. Huang, C. Zhang, Ag–TiO_2–Ag core–shell-satellite nanowires: facile synthesis and enhanced photocatalytic activities, Materials Letters 80 (2012) 138–140.
[8] S. Cheewita, W. Sumpun, S. Pimpaporn, M. Pachara, Enhancement of the photocatalytic performance of Ag-modified TiO_2 photocatalyst under visible light, Ceramics International 38 (2012) 5201–5207.
[9] T. Hakoda, K. Matsumoto, A. Mizuno, K. Hirota, Role of metals loaded on a TiO_2 surface in the oxidation of xylene in air using an electron beam irradiation/catalytic process, Applied Catalysis A: General 357 (2009) 244–249.
[10] S. Sun, J.J. Ding, J. Bao, C. Gao, Z.M. Qi, X.Y. Yang, B. He, C.X. Li, Photocatalytic degradation of gaseous toluene on Fe–TiO_2 under visible light irradiation: A study on the structure, activity and deactivation mechanism, Applied Surface Science 258 (2012) 5031–5037.
[11] N. Riaz, F.K. Chong, B.K. Dutta, Z.B. Man, M.S. Khan, E. Nurlaela, Photodegradation of orange II under visible light using Cu–Ni/TiO_2: Effect of calcination temperature, Chemical Engineering Journal. 185–186 (2012) 108–119.

[12] T. Nogawa, T. Isobe, S. Matsushita, A. Nakajima, Preparation and visible-light photocatalytic activity of Au- and Cu-modified TiO_2 powders, Materials Letters 82 (2012) 174–177.
[13] Y.H. Peng, G.F. Huang, W.Q. Huang, Visible-light absorption and photocatalytic activity of Cr-doped TiO_2 nanocrystal films, Advanced Powder Technology 23 (2012) 8–12.
[14] Q.R. Deng, X.H. Xia, M.L. Guo, Y. Gao, G. Shao, Mn-doped TiO_2 nanopowders with remarkable visible light photocatalytic activity, Materials Letters 65 (2011) 2051–2054.
[15] M. Bellardita, M. Addamo, A. Di Paola, L. Palmisano, Photocatalytic behaviour of metal-loaded TiO_2 aqueous dispersions and films, Chemical Physics 339 (2007) 94–103.
[16] H.C. He, P. Xiao, M. Zhou, Y.H. Zhang, Q. Lou, X.Z. Dong, Boosting catalytic activity with a p–n junction: Ni/TiO_2 nanotube arrays composite catalyst for methanol oxidation, International Journal of Hydrogen Energy 37 (2012) 4967–4973.
[17] S. Onsuratoom, T. Puangpetch, S. Chavadej, Comparative investigation of hydrogen production over Ag-, Ni-, and Cu-loaded mesoporous-assembled TiO_2–ZrO_2 mixed oxide nanocrystal photocatalysts, Chemical Engineering Journal 173 (2011) 667–675.
[18] Y.H. Zhang, Y.N. Yang, P. Xiao, X.N. Zhang, L. Lu, L. Li, Preparation of Ni nanoparticle-TiO_2 nanotube composite by pulse electrodeposition, Materials Letters 63 (2009) 2429–2431.
[19] B.I. Stefanov, N.V. Kaneva, G.L. Puma, C.D. Dushkin, Novel integrated reactor for evaluation of activity of supported photocatalytic thin films: Case of methylene blue degradation on TiO_2 and nickel modified TiO_2 under UV and visible light, Colloids and Surfaces A 382 (2011) 219–225.
[20] Z.J. Wu, J. Chen, Q. Di, M.H. Zhang, Size-controlled synthesis of a supported Ni nanoparticle catalyst for selective hydrogenation of p-nitrophenol to p-aminophenol, Catalysis Communications 18 (2012) 55–59.
[21] M.I. Zaki, G.A.H. Mekhemer, N.E. Fouad, T.C. Jagadale, S.B. Ogale, Surface texture and specific adsorption sites of sol–gel synthesized anatase TiO_2 nanoparticles, Materials Research Bulletin 45 (2010) 1470–1475.
[22] K. Karthik, S.K. Pandian, N.V. Jaya, Effect of nickel doping on structural, optical and electrical properties of TiO_2 nanoparticles by sol–gel method, Applied Surface Science 256 (2010) 6829–6833.
[23] S.X. Liu, Z.P. Qu, X.W. Han, C.L. Sun, X.H. Bao, Effect of silver deposition on photocatalytic activity of TiO_2, Chinese Journal of Catalysis 25 (2004) 133–137.
[24] P. Christopher, D.B. Ingram, S. Linic, Enhancing photochemical activity of semiconductor nanoparticles with optically active Ag nanostructures: photochemistry mediated by Ag surface plasmons, Journal of Physical Chemistry C 114 (2010) 9173–9177.